Supplementary Figures

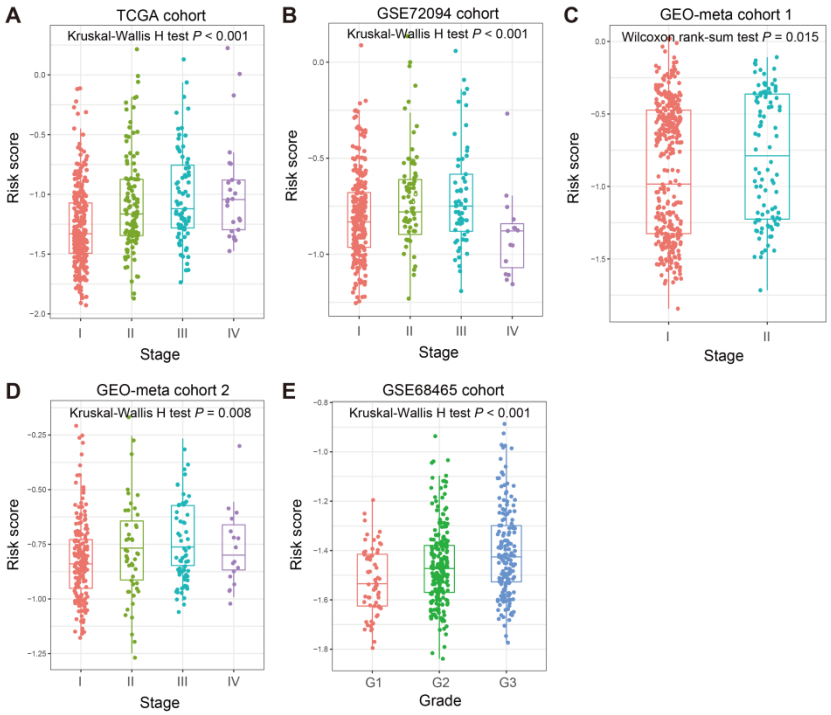

Figure S1. Distribution of the identified aging risk signature scores in distinct clinical stages or histology grade under (A) TCGA, (B) GSE72094, (C) GEO-meta cohort 1, (D) GEO-meta cohort 2, and (E) GSE68465 cohorts.

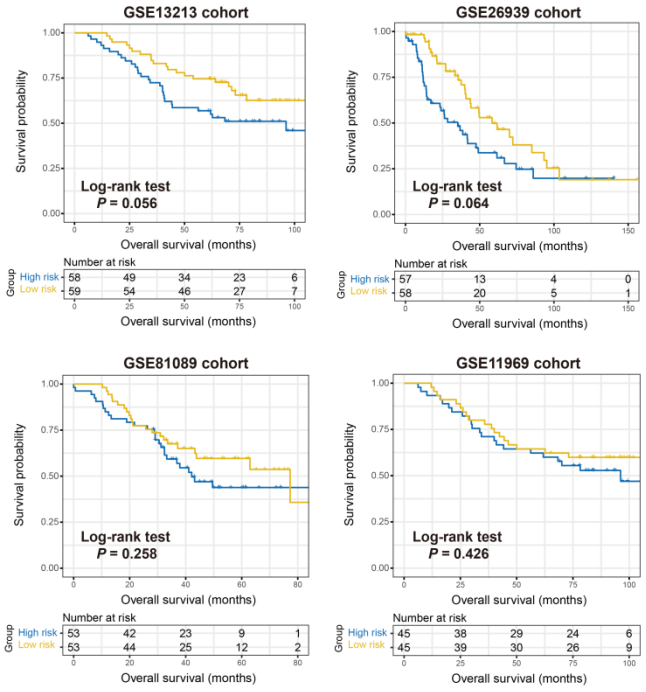

Figure S2. Kaplan-Meier survival curves stratified by patients of distinct risk levels in (A) GSE13213, (B) GSE26939, (C) GSE81089, and (D) GSE11969 cohorts.

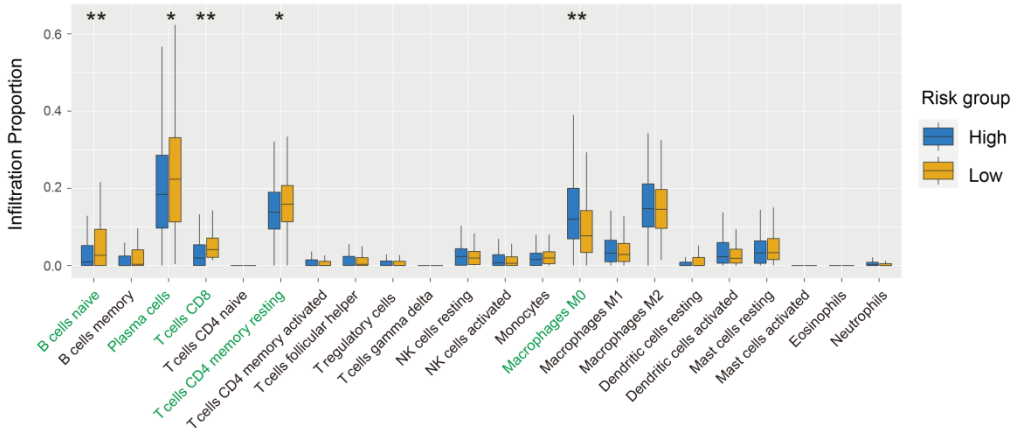

Figure S3. Abundance of distinct tumor infiltrating immune cells in low- versus high-risk subgroups evaluated by CIBERSORT algorithm. Immunocyte highlighted with green was significantly differentially infiltrated between two LUAD risk subgroups. * $P < 0.05$, ** $P < 0.01$

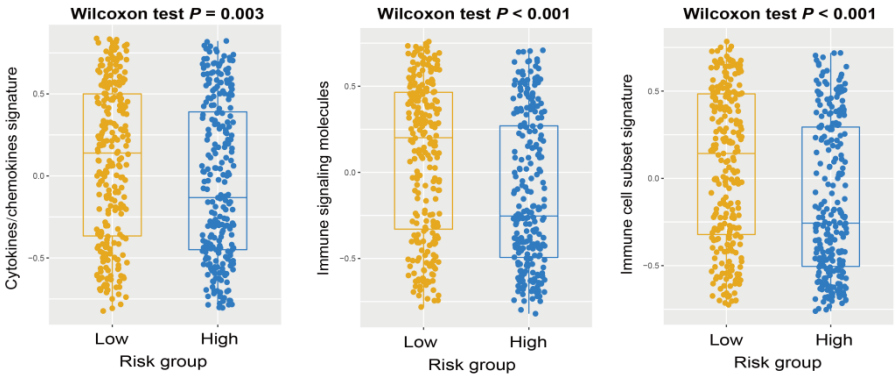

Figure S4. Distinct enrichment distribution of cytokines/chemokines signature, immune signaling molecules, and immune cell subset signature in low- and high-risk LUAD patients.

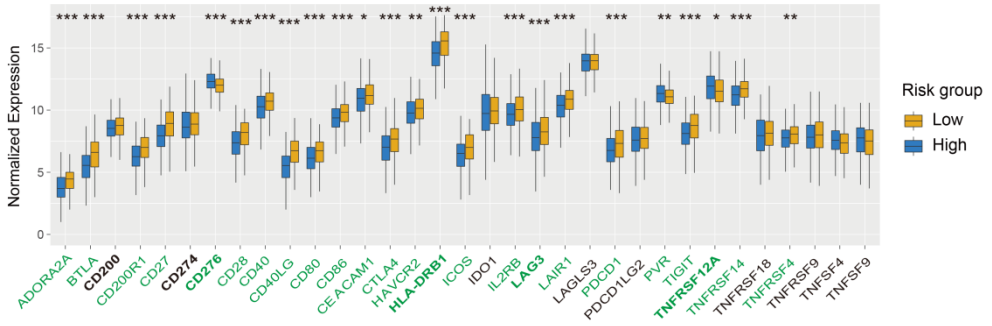

Figure S5. Distinct expression of 33 immune checkpoint genes in low- versus high-risk LUAD patients. Genes highlighted with green were significantly differentially expressed between two groups. * $P < 0.05$, ** $P < 0.01$, *** $P < 0.001$

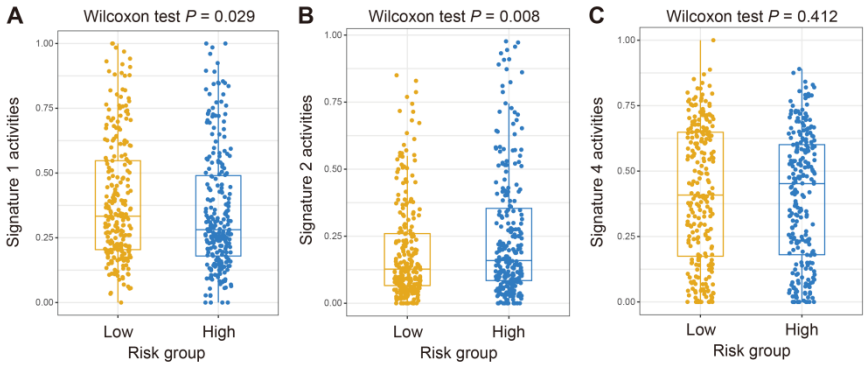

Figure S6. Mutational activity distribution of (A) signature 1, (B) signature 2, and (C) signature 4 in low- and high-risk subgroups.

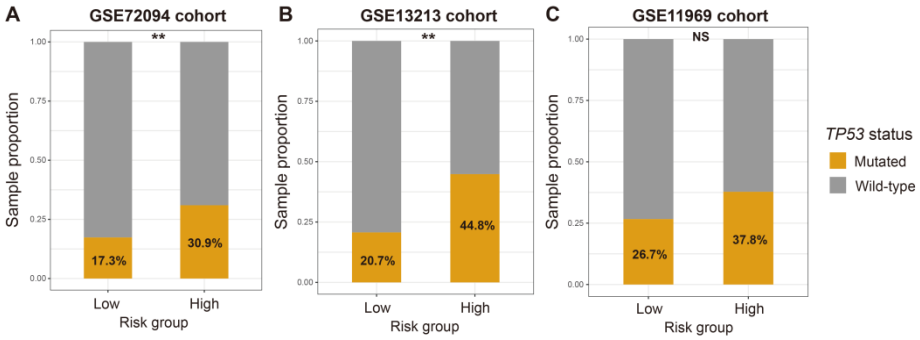

Figure S7. Associations of aging risk signature with *TP53* mutation rate in (A) GSE72094, (B) GSE13213, and (C) GSE11969 cohorts.

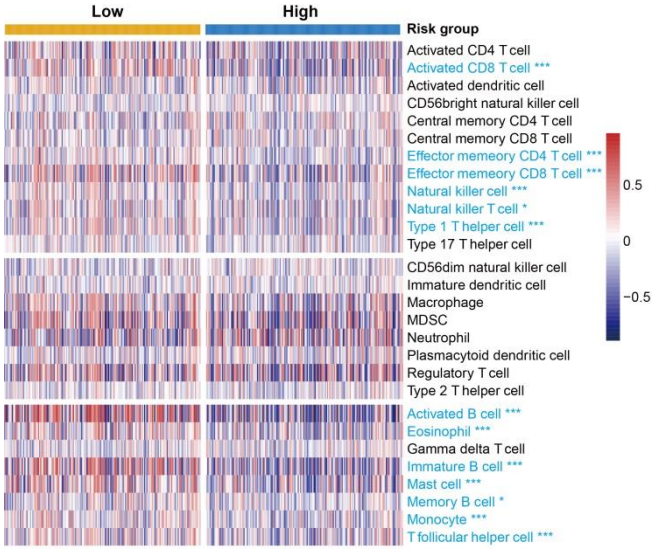

Figure S8. Heatmap representation of distinct immunocyte infiltration in two risk subpopulations under the genomic data from the urothelial cancer ICI cohort. Immunocyte highlighted with blue indicated its infiltration was significantly elevated in low-risk patients.

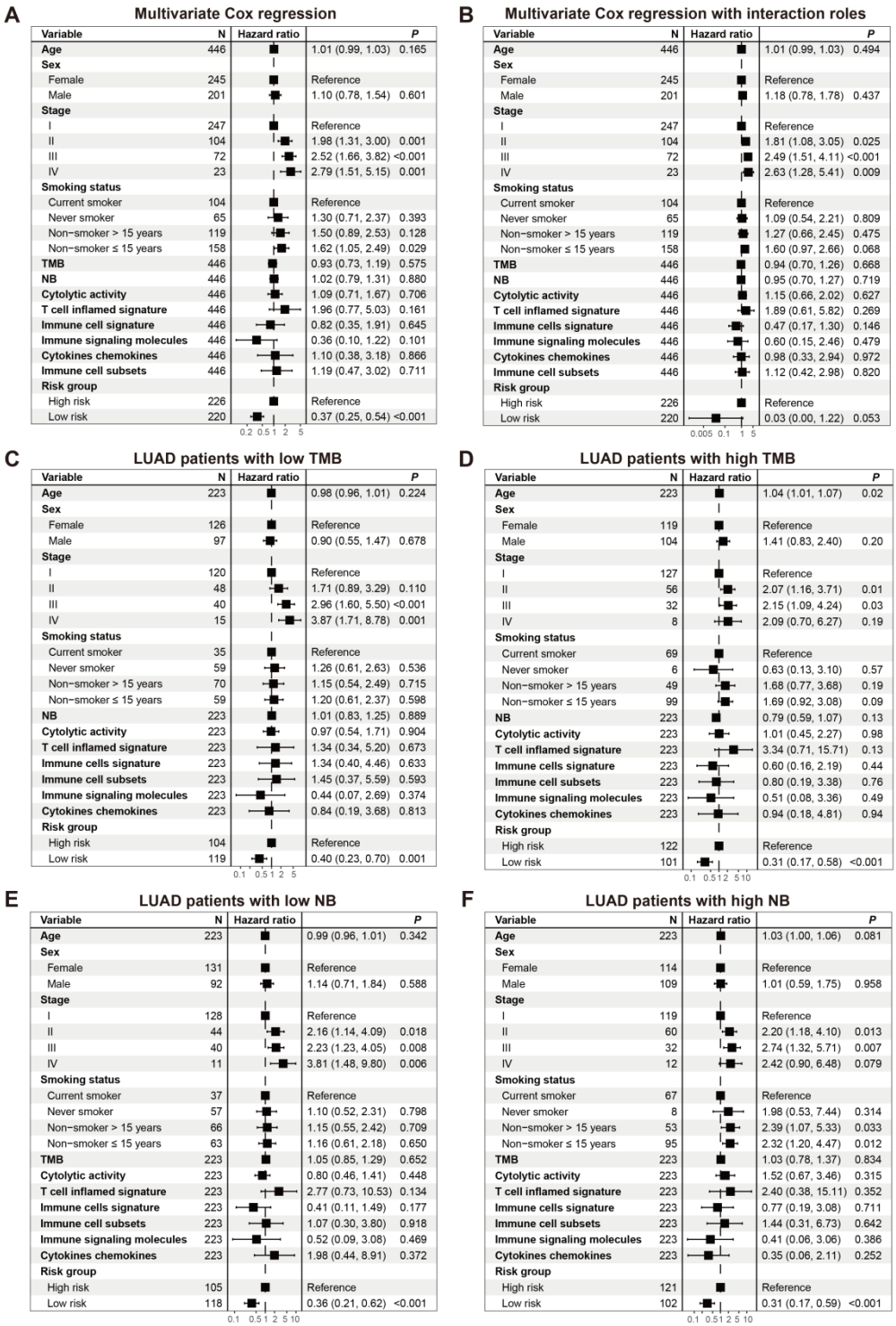

Figure S9. (A) Multivariate Cox regression model, (B) interaction role analyses, and (C, D, E, F) stratification analyses based on the mutational burden were conducted to elucidate the association between the aging risk signature and LUAD survival outcome.